THE JOURNAL OF PHYSICAL CHEMISTRY LETTERS
A JOURNAL OF THE AMERICAN CHEMICAL SOCIETY

pubs.acs.org/JPCL

Letter

Counterintuitive Catalytic Reactivity of the Aluminum Oxide "Passivation" Shell of Aluminum Nanoparticles Facilitating the Thermal Decomposition of *exo*-Tetrahydrodicyclopentadiene (JP-10)

Souvick Biswas, Dababrata Paul, Chao He, Nureshan Dias, Musahid Ahmed,* Michelle L. Pantoya,* and Ralf I. Kaiser*

Cite This: *J. Phys. Chem. Lett.* 2023, 14, 9341−9350

Read Online

ACCESS | Metrics & More | Article Recommendations | Supporting Information

ABSTRACT: High energy density aluminum nanoparticles (AlNPs) have been at the center of attention as additives to hydrocarbon jet fuels like *exo*-tetrahydrodicyclopentadiene (JP-10, $C_{10}H_{16}$) aiming at the superior performance of volume-limited air-breathing propulsion systems. However, a fundamental understanding of the ignition and combustion chemistry of JP-10 in the presence of AlNPs has been elusive. Exploiting an isomer-selective comprehensive identification of the decomposition products in a newly designed high-temperature chemical microreactor coupled to vacuum ultraviolet photoionization, we reveal an active low-temperature heterogeneous surface chemistry commencing at 650 K involving the alumina (Al_2O_3) shell. Contrary to textbook knowledge of an "inactive alumina surface", this unconventional reactivity, where oxygen is transferred from alumina to JP-10, leads to generating cyclic, oxygenated organics like phenol (C_6H_5OH) and 2,4-cyclopentadiene-1-one (C_5H_4O)—key tracers of an alumina-mediated interfacial chemistry. This counterintuitive reactivity transforms our knowledge of the (catalytic) processes of alumina-coated AlNPs on the molecular level.

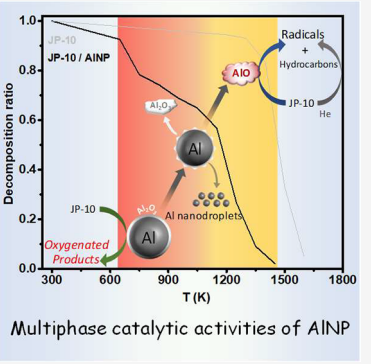

During the past decade, high energy density aluminum nanoparticles (AlNPs) with a remarkable volumetric energy density of 84.3 kJ cm^{-3} have received widespread attention as affordable and efficient additives to single-component hydrocarbon jet fuels such as *exo*-tetrahydrodicyclopentadiene (JP-10, $C_{10}H_{16}$) aiming at a superior performance of volume-limited air-breathing propulsion systems.[1−12] Intrinsically, these materials offer key advantages as AlNPs provide higher specific surface areas, reduce ignition delays, enhance the heat transfer rate, and boost the volumetric energy densities of traditional hydrocarbon fuels (35−40 kJ cm^{-3}).[6,7] These benefits in turn enable enhanced flight ranges of aircraft.[13−19] In strong contrast to micrometer-sized aluminum particles, nanometer-sized aluminum particles burn heterogeneously rather than via vapor-phase oxidation, thereby bringing the flame toward the surface of the particle and decreasing the diffusion length.

However, fundamental knowledge of the ignition and combustion chemistry of JP-10 in the presence of AlNPs is still in its infancy. These processes have been suggested to be multistaged considering the presence of a presumed inert aluminum oxide (Al_2O_3) passivation layer[20−23] surrounding the metallic aluminum core.[24] Recent studies proposed that the aluminum oxide shell might have a catalytic potential in the presence of fluorocarbons.[21,25,26] Padhye et al. performed density function theory calculations for a fluorinated hydrocarbon species and suggested an exoergic interaction between terminal hydroxyl bonds on the oxide surface layer of AlNPs and fluoromethane (CH_3F).[26] Suspending AlNPs in JP-10 extends this picture.[11,12,27] A transformation of the oxide shell into an exoergic energy contributor could significantly impact energy generation technologies. Preliminary studies reported a two-phase model with an early burning of the fuel itself followed by a rupture of the oxide shell and aluminum combustion.[4,5,28] However, a prior fracture of the aluminum oxide shell was proposed for combustion of AlNP-doped JP-10 droplets at temperatures of about 2600 K facilitating the generation of carbon-centered radicals via hydrogen transfer from chemically distinct carbon−hydrogen (C−H) bonds of JP-10 to the reactive surface of the aluminum core. The successive oxidation of these organic radical intermediates completes the combustion process.[10−12]

These conflicting studies of AlNP/JP-10 fuel suggest that a complete chemical and physical understanding at the molecular level of the role of AlNP additives along with their oxide layer in the presence of JP-10 has remained highly

Received: September 9, 2023
Accepted: September 29, 2023

https://doi.org/10.1021/acs.jpclett.3c02532
J. Phys. Chem. Lett. 2023, 14, 9341−9350

ambiguous. Molecular information on the initial steps to *chemically activate* JP-10 in the presence of AlNPs through the generation of radicals and the determination of the complex inventory of reactive inorganic and organic transient species along with stable molecules are not available. These radical species deliver the building blocks for the oxidation of JP-10 at a later stage of the oxidation, thus controlling the overall efficiency and performance of combustion. Finally, the catalytic role of the presumed inert aluminum oxide layer in the decomposition and combustion process has remained largely obscure. The unraveling of this knowledge is critical for the design of AlNP/JP-10-supported next-generation hypersonic propulsion systems and the fundamental processes which control the decomposition of organic molecules in the presence of oxides and metal nanoparticles.

Here, we report for the very first time a detailed mechanistic picture of alumina-coated AlNPs in the thermal decomposition of JP-10 at combustion-relevant temperatures through the isomer-selective identification of the temperature-dependent decomposition products in a newly designed chemical microreactor (Scheme 1) exploiting vacuum ultraviolet single photon ionization of the radicals and closed-shell molecules (Supporting Information, Section S1).

Scheme 1. Thermal Decomposition of JP-10 Explored in a High-Temperature Chemical Microreactor (Hot Silicon Carbide (SiC) Tube) through a Compact Packing of 80 nm Sized Alumina (Al_2O_3) Coated Aluminum Nanoparticles (AlNPs)[a]

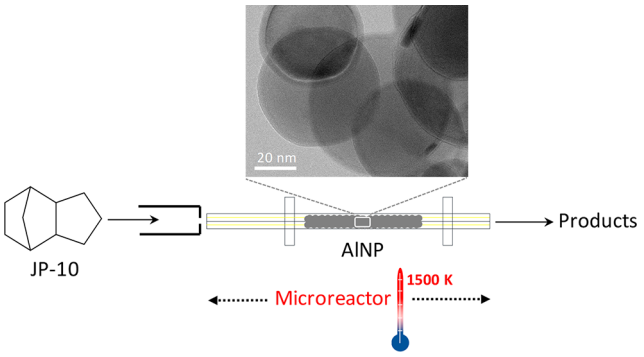

[a]A transmission electron microscopy (TEM) image of the AlNP showing the Al_2O_3 shell is shown in the inset.

These experiments reveal an *active heterogeneous surface chemistry* of the previously assumed "inert" oxide layer of the AlNPs not only in the thermal decomposition but also in the oxidation of JP-10. The initial oxidation of JP-10 over AlNPs commences at 550 K *lower* than that of helium-seeded JP-10,[29] starting at 650 K. The quantitative decomposition of JP-10 was observed at 1450 K, which is 150 K lower than that of helium-seeded JP-10. The oxide layer *actively participates* in the oxidation of JP-10 molecules by transferring oxygen to JP-10 and its radicals, producing low-temperature, primarily cyclic oxidation products such as phenol (C_6H_5OH), cresol ($CH_3C_6H_4OH$), benzyl alcohol ($C_6H_5CH_2OH$), dimethylphenol ($(CH_3)_2C_6H_3OH$), and 2,4-cyclopentadiene-1-one (C_5H_4O). Our findings challenge conventional understanding that the previously assumed "inert", chemically nonreactive oxide layer of AlNPs blocks an efficient oxidation of organic fuels and AlNPs themselves, whereas the experimental observations herein provide compelling evidence for a chemically active oxide layer initiating a facile low-temperature decomposition of JP-10 eventually leading to an unconventional route to oxygenated JP-10 fragments over AlNPs. These results provide a fundamental, previously elusive mechanistic understanding of the (catalytic) role of the oxide layers of AlNPs in the oxidation of organic fuel such as JP-10, ultimately leading to the development of advanced air-breathing ramjet and scramjet systems with superior volumetric energy release.

Mass Spectra. The experiments were conducted in a chemical microreactor[29−31] (Figure S3) by passing helium-seeded *exo*-tetrahydrodicyclopentadiene (JP-10, $C_{10}H_{16}$) over AlNPs at distinct temperatures from 300 K to 1450 K. The nascent gas-phase products are entrained in a supersonic molecular beam and probed *in situ* with soft photoionization with *isomer selective* single photon vacuum ultraviolet (VUV) ionization followed by a mass analysis of the generated ions in a reflectron time-of-flight mass spectrometer (Re-TOF-MS).[32] By scanning the photon energy from 8.0 to 10.5 eV and extracting photoionization efficiency (PIE) curves for distinct mass-to-charge (m/z) ratios, this technique affords an *isomer-selective* identification of both closed-shell species and radical transients.[29] At definite intervals of the experimental temperature range, characteristic mass spectra recorded at a photon energy of 10.0 eV are compiled (Figure 1A). At 300 K, the mass spectrum depicts only two peaks of the molecular parent ion at m/z = 136 ($C_{10}H_{16}^+$) and of the ^{13}C counterpart at m/z = 137 ($^{13}CC_9H_{16}^+$). The JP-10 decomposition ratios flowing through the high-temperature chemical microreactor with and without AlNPs are depicted in Figure 1B.

Thirteen additional ion counts appear at m/z = 58, 66, 67, 68, 69, 80, 81, 94, 95, 107, 108, 121, and 122 at 650 K. With the rise of the temperature to 1450 K, the number of mass peaks increases to fifty-four, thus indicating a critical role of temperature in the formation of new products. It is important to highlight that no signal was observed at m/z values exceeding 136 ($C_{10}H_{16}^+$) and 137 ($^{13}CC_9H_{16}^+$); this finding confirms the lack of molecular mass growth processes, which is a necessary requirement to investigate only the decomposition and/or oxidation products of individual JP-10 molecules in our experimental setup. In tandem with the rising complexity of the mass spectrum with increasing temperature, the intensity of the molecular parent peak of JP-10 at m/z = 136 ($C_{10}H_{16}^+$) decreases sharply (Figure 1B; red trace). The presence of AlNPs results in a significant earlier onset of decomposition of JP-10 at 650 K (red trace) compared to 1200 K without AlNPs (black trace).[29] Furthermore, the complete decomposition of JP-10 occurred at 1450 K, i.e., 150 K lower than without AlNPs under otherwise identical experimental conditions. Overall, the presence of AlNPs essentially shifts the decomposition curve to lower-temperature regions having distinct slopes in the range of 1150−1450 K and 650−1150 K revealing a critical influence of the nanoparticles on the decomposition and/or oxidation of JP-10.

Photoionization Efficiency (PIE) Curves. To achieve an understanding of the effects of AlNPs on the decomposition and oxidation of JP-10 at the molecular level, it is imperative to identify the nature of the decomposition and oxidation products entrained in the molecular beam. This is accomplished through an extraction and detailed analysis of distinct PIE curves and a comparison of the JP-10/AlNP system with the helium-seeded pure JP-10 reference system.[29] Overall, 57 products (Table S1) were identified in this study[33−42] which can be categorized into four groups: (i) oxygenated closed-

https://doi.org/10.1021/acs.jpclett.3c02532
J. Phys. Chem. Lett. 2023, 14, 9341−9350

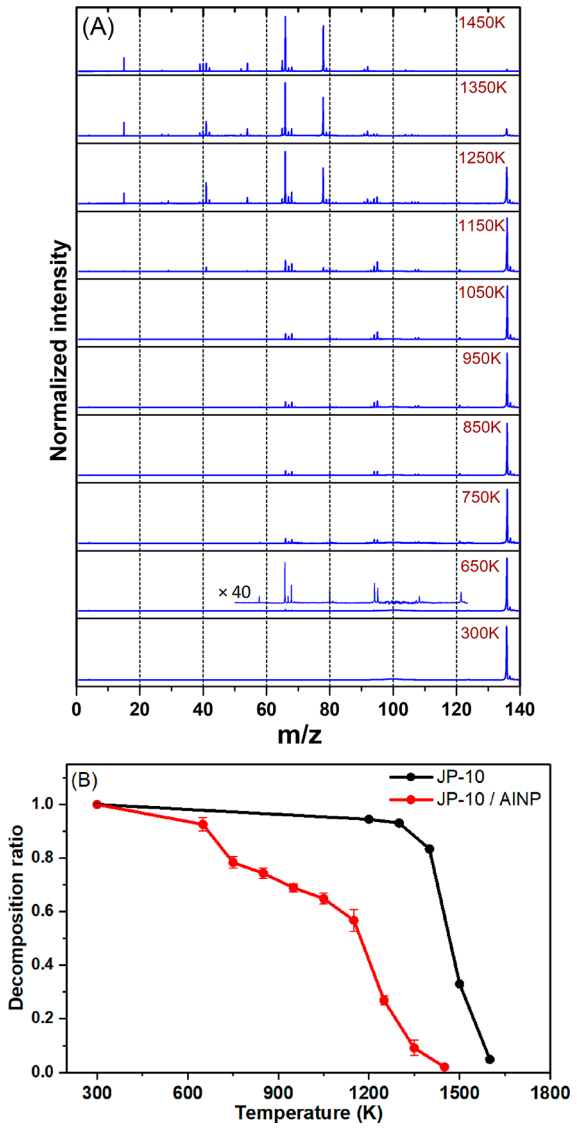

Figure 1. (A) Mass spectra of the products formed upon thermal decomposition of JP-10 through a packing of aluminum nanoparticles (AlNPs) recorded at a photon energy of 10.0 eV in the 300−1450 K temperature range. (B) Decomposition ratios for JP-10 passing through the high-temperature chemical microreactor with (red trace) and without (black trace) AlNPs.

shell molecules, (ii) oxygenated radicals, (iii) closed-shell hydrocarbons (Figure S4), and (iv) hydrocarbon radicals. Considering the absence of any external supply of molecular oxygen, the detection of the oxygenated products alone provides compelling evidence on an active chemistry and hence oxygen supply from the aluminum oxide layer (Al_2O_3).

Oxygenated Molecules. At 650 K, the oxidized products (Figure 2A), such as acetone (CH_3COCH_3, m/z = 58), propanal ($HCOC_2H_5$, m/z = 58), furan (C_4H_4O, m/z = 68), 2,4-cyclopentadiene-1-one (C_5H_4O, m/z = 80), phenol (C_6H_5OH, m/z = 94), cresol ($CH_3C_6H_4OH$, m/z = 108), benzyl alcohol ($C_6H_5CH_2OH$, m/z = 108), and dimethylphenol ($(CH_3)_2C_6H_3OH$, m/z = 122), started to form, except benzaldehyde (C_6H_5CHO, m/z = 106) which was obtained at 1050 K and higher temperatures. Water (IE = 12.6 eV),[43] a classical combustion product, was also detected in the mass spectra recorded at 15.4 eV (Figure S5); however, no carbon dioxide (CO_2, IE = 13.8 eV)[44] was observed.

Oxygenated Radicals. Phenoxy ($C_6H_5O^\bullet$, m/z = 93), methylphenoxy ($CH_3C_6H_4O^\bullet$, m/z = 107), and dimethylphenoxy ($(CH_3)_2C_6H_3O^\bullet$, m/z = 121) radicals are detected at 650 K along with the oxygenated molecules. However, the formyl ($HCO^\bullet$, m/z = 29) and ethynyloxy ($HCCO^\bullet$, m/z = 41) radicals form at elevated temperatures beyond 1050 K (Figure 2(A)). Since no literature PIE curves are available for the methylphenoxy ($CH_3C_6H_4O^\bullet$) and dimethylphenoxy radicals ($(CH_3)_2C_6H_3O^\bullet$), these species are assigned based on the onset of the ion counts and hence the adiabatic ionization energy (IE) of the former.[40,42] The signal at m/z = 96 can be tentatively assigned to 2-cyclohexen-1-one (C_6H_8O, IE = 9.23 eV).[45] Besides these organic molecules, our studies also provided persuasive testimony on the presence of aluminum monoxide (AlO, IE = 9.6 eV)[46] at m/z = 43, once again ensuring an active participation of the oxide layer. It is important to highlight that the PIE curve at m/z = 43 cannot be replicated with the known reference PIE curve of the 1- and/or 2-propyl radicals ($^\bullet C_3H_7$; IE = 8.1 and 7.4 eV).

Hydrocarbon Molecules. Although at the initiation of the decomposition of JP-10 at 650 K, the major hydrocarbon product is identified as *1,3-cyclopentadiene* (C_5H_6, IE = 8.5 eV), with rising temperature beyond 1050 K, a complex pool of closed-shell hydrocarbons emerged (Figure S4), namely: *acetylene* (HC≡CH, IE = 11.4 eV), *ethylene* ($H_2C=CH_2$, IE = 10.5 eV), *allene* ($H_2C=C=CH_2$, IE = 9.7 eV), *methylacetylene* ($CH_3—C\equiv CH$, IE = 10.4 eV), *propene* ($CH_3—CH=CH_2$, IE = 9.7 eV), *diacetylene* ($HC\equiv C—C\equiv CH$, IE = 10.1 eV), *vinylacetylene* ($H_2C=CH—C\equiv CH$, IE = 9.6 eV), *1,3-butadiene* ($H_2C=CH—CH=CH_2$, IE = 9.1 eV), *1-butene* ($H_3C—CH_2—CH=CH_2$, IE = 9.6 eV), *ethynylallene* ($HC\equiv C—CH=C=CH_2$, IE = 9.2 eV), *benzene* (C_6H_6, IE = 9.2 eV), *fulvene* (C_6H_6, IE = 8.4 eV), *5-ethenylidene-1,3-cyclopentadiene/fulvenallene* (C_7H_6, IE = 8.3 eV), *toluene* (C_7H_8, IE = 8.8 eV), *5-methylene-1,3-cyclohexadiene* (C_7H_8, IE = 7.9 eV), *phenylacetylene* (C_8H_6, IE = 8.8 eV), *benzocyclobutadiene* (C_8H_6, IE = 7.5 eV), *styrene* (C_8H_8, IE = 8.4 eV), *p*-xylene (C_8H_8, IE = 8.5 eV), *1,3,5-cyclooctatriene* (C_8H_{10}, IE = 7.9 eV), *indene* (C_9H_8, IE = 8.3 eV), 1-ethynyl-4-methylbenzene (C_9H_8, IE = 8.5 eV), and *indane* (C_9H_{10}, IE = 8.6 eV). Those hydrocarbons indicated in *italics* were also detected in the decomposition of helium-seeded JP-10,[29] but only at temperatures of 1200 K and beyond. Herein, the detection of molecular hydrogen (Figure S5) may benefit the ignition and combustion under hypersonic conditions by acting as a functional heat sink.[47]

Hydrocarbon Radicals. As a general trend, hydrocarbon radicals form in noticeable amounts at higher temperatures exceeding 1150 K (Figure 2(B)). The major species are *methyl* ($^\bullet CH_3$, IE = 9.8 eV), *vinyl* ($^\bullet CH=CH_2$, IE = 8.3 eV), *propargyl* ($^\bullet CH_2—C\equiv CH$, IE = 8.7 eV), *allyl* ($^\bullet CH_2—CH=CH_2$, IE = 8.1 eV), *cyclopentadienyl* ($^\bullet C_5H_5$, IE = 8.4 eV), and benzyl ($^\bullet C_7H_7$, IE = 7.2 eV). Among these, the benzyl radical was not detected during the pyrolysis of helium-seeded JP-10.[29]

Temperature-Dependent Product Yields. The temperature-dependent abundances along with their branching ratios allow an extraction of the underlying mechanisms of the oxidation and decomposition pathways of JP-10 over AlNPs. The normalized intensities of key species are depicted for the temperature range from 650 to 1450 K in Figure 3, while

https://doi.org/10.1021/acs.jpclett.3c02532
J. Phys. Chem. Lett. 2023, 14, 9341−9350

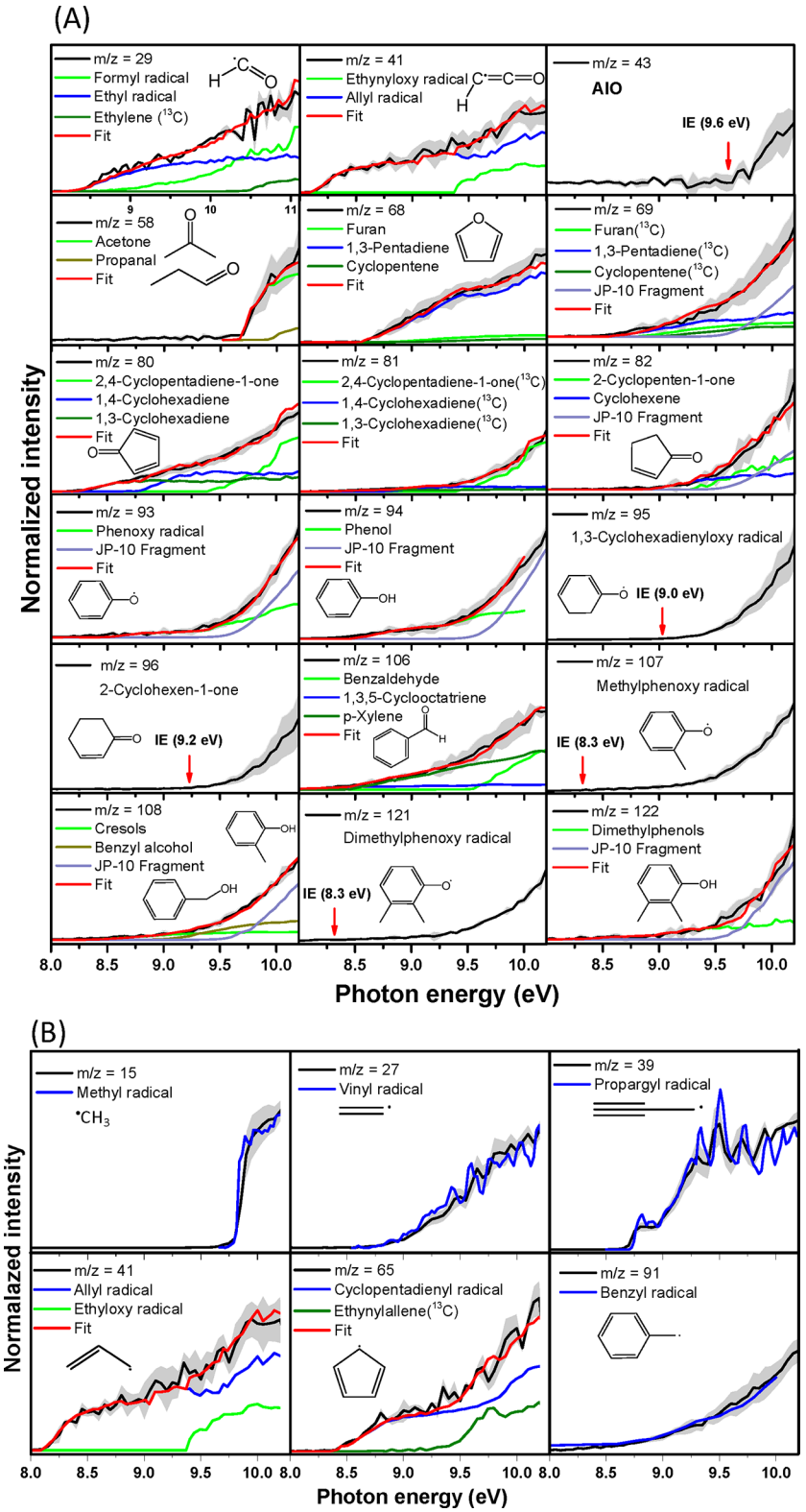

Figure 2. Experimental photoionization efficiency curves (PIE, black traces) for the (A) oxygenated (green reference traces) and (B) radical products (blue reference traces) formed upon thermal decomposition of JP-10 by aluminum nanoparticles (AlNPs) along with the experimental errors (gray shaded area) originating from the measurement errors of the photocurrent by the photodiode and a 1-σ error of the PIE curves averaged over the individual scans. In the case of multiple isomeric contributions, individual reference PIE curves are presented and the overall fitted curve is depicted by the red trace. JP-10 fragment implies the photolysis fragment of JP-10 generated upon dissociative photoionization.

overall branching ratios are visualized in Figure 4 by accounting for the photoionization cross sections. First, considering the oxidized products (Figure 3, Figure S6), a general pattern emerges with bell-shaped temperature-dependent yields with maxima observable in the temperature range of 1050−1250 K; oxygenated radicals carrying the (hydro-

https://doi.org/10.1021/acs.jpclett.3c02532
J. Phys. Chem. Lett. 2023, 14, 9341−9350

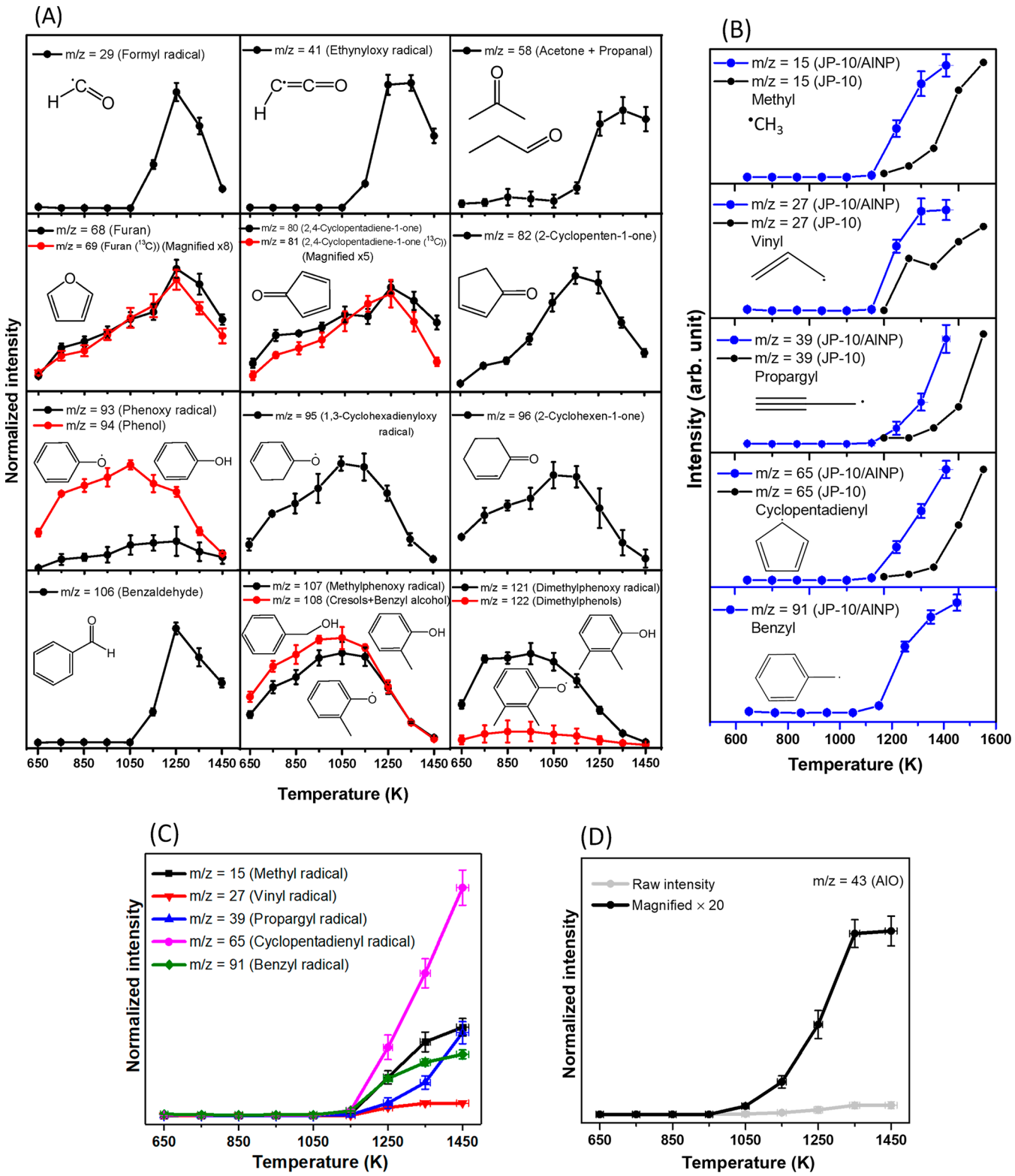

Figure 3. Temperature-dependent (A) abundances of oxygenated products and (B) comparison between the abundances of the hydrocarbon radicals formed upon thermal decomposition of JP-10 with aluminum nanoparticles (AlNPs) (blue trace) and without AlNPs (black trace) along with the plot of relative peak intensities at the normalized scale for the (C) hydrocarbon radicals and (D) aluminum monoxide (AlO) as products due to pyrolysis of JP-10 by AlNPs. The *y*-error bars are due to the experimental errors of the mass peak intensities evaluated by averaging recorded mass spectra at 10 eV, while the *x*-error bars are associated with the measurement errors of the temperature of the microreactor.

genated) benzene ring such as in the phenoxy ($C_6H_5O^•$), 1,3-cyclohexadienyloxy ($C_6H_7O^•$), methylphenoxy ($C_7H_7O^•$), and dimethylphenoxy radical ($C_8H_9O^•$) already emerge at temperatures as low as 650 K, thus highlighting a facile oxidation process in the absence of AlNPs; recall that helium-seeded JP-10 in the absence of AlNPs did not decompose at 650 K.[29]

https://doi.org/10.1021/acs.jpclett.3c02532
J. Phys. Chem. Lett. 2023, 14, 9341−9350

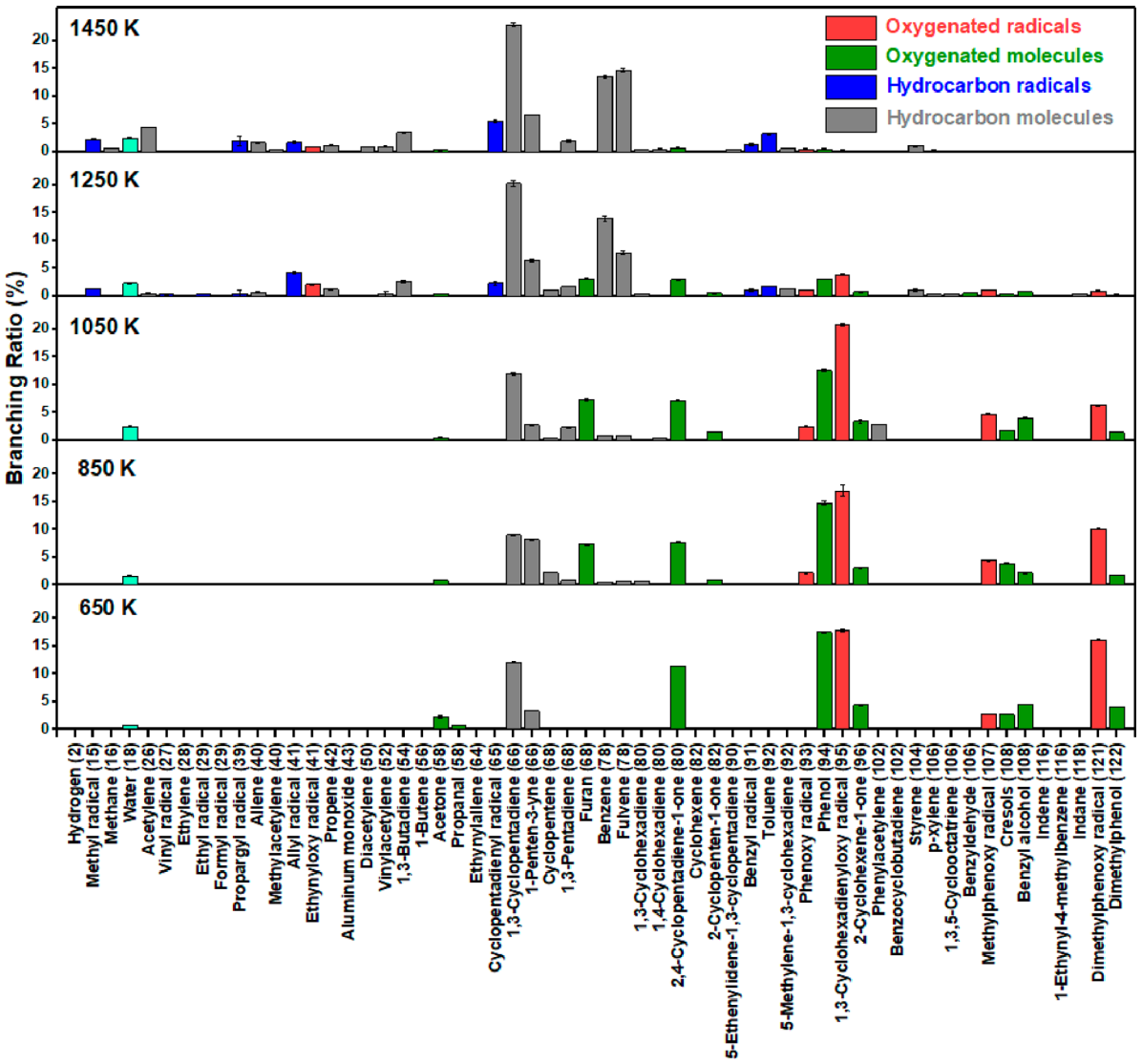

Figure 4. Overall branching ratios of the species obtained in the thermal decomposition of JP-10 by aluminum nanoparticles (AlNPs) in the temperature range from 650 to 1450 K. The error bars are evolved due to the uncertainties determined by averaging the recorded photoionization efficiency curves.

Overall, the major products obtained are furan (C_4H_4O, 7.3 ± 0.2%), 2,4-cyclopentadiene-1-one (C_5H_4O, 7.2 ± 0.2%), phenol (C_6H_5OH, 12.6 ± 0.3%), 1,3-cyclohexadienyloxy ($C_6H_7O^•$, 20.9 ± 0.2%), and the dimethylphenoxy radical ($(CH_3)_2C_6H_3O^•$, 6.4 ± 0.1%) at 1050 K.

Second, the temperature-dependent pattern of the hydrocarbon radicals (Figure 3B,C) is quite distinct from the oxygenated products (Figure 3A). Here, formation of the hydrocarbon radicals commences at elevated temperatures from 1150 K. However, the yields of the oxygenated radicals decline with rising temperature, while those of the hydrocarbon radicals essentially increase up to the highest temperature of 1450 K. Similar to the decomposition curve of JP-10 (Figure 1B), the temperature-dependent radical yields are shifted toward lower temperature in the presence of AlNPs. At 1450 K, the cyclopentadienyl radical ($^•C_5H_5$) was found to be the major contributor (5.5 ± 0.3%) followed by methyl ($^•CH_3$, 2.2 ± 0.1%) and propargyl ($^•C_3H_3$, 2.0 ± 0.8%). The dominant hydrocarbon products are 1,3-cyclopentadiene (C_5H_6, 20.3 ± 0.6%), benzene (C_6H_6, 13.9 ± 0.5%), and its isomer fulvene (C_6H_6, 7.8 ± 0.3%) at 1250 K; the benzene-to-fulvene isomerization is favored at 1450 K as reflected from the enhancement of the fulvene-to-benzene ratio of 0.6 ± 0.2% versus 1.1 ± 0.4%. Third, the production of aluminum monoxide (AlO) commences at about 950 K and increases monotonically as the temperature rises to 1450 K. The overall carbon-to-hydrogen (C/H) ratio calculated for the temperature range of 650−1450 K remains unchanged quantitatively as depicted in Figure 5A. This demonstrates mass conservation in the product distribution and, as a result, thorough detection of the products. The temperature-dependent oxygen uptake coefficients to oxygenated products are shown in Figure 5B. Given that the oxygen incorporated into the oxygenated products can originate only from the aluminum oxide layer, the uptake coefficient (Supporting Information, Section S2) reveals a maximum oxygen atom transfer efficiency of 0.44 ± 0.09 at 1050 K, which correlates with a peaking of the yields of the oxygenated products at that temperature (Figure 3A).

The aforementioned findings suggest that the presence of AlNPs exhibits at least three distinct oxidation and decomposition regimes of JP-10 with multifaceted reaction pathways involving the aluminum oxide surface and the gas-

https://doi.org/10.1021/acs.jpclett.3c02532
J. Phys. Chem. Lett. 2023, 14, 9341−9350

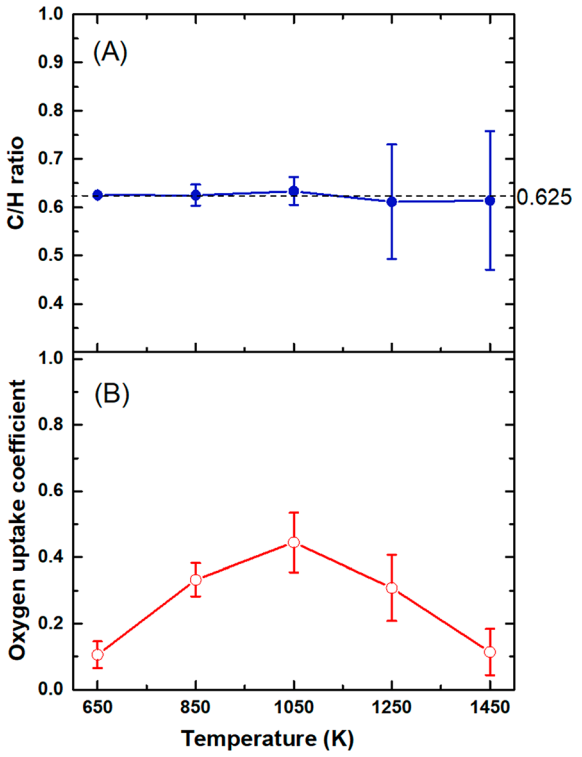

Figure 5. (A) The C/H ratio for the pyrolysis of JP-10 by aluminum nanoparticles (AlNPs) in the temperature range from 650 to 1450 K. The dashed line represents the expected ratio maintaing the mass balance. (B) Temperature-dependent oxygen uptake coefficients from aluminum oxide shell to oxygenated molecules and radicals. The errors consist of the errors generated in the calculation of branching ratios of the products and quantification of the alumina (Al_2O_3) content in the aluminum nanoparticles (AlNPs).

phase AlO radical: a **low-temperature oxidation regime** (650−1050 K) driven by an aluminum oxide surface-mediated oxidation of JP-10, a **medium-temperature regime** (1050−1250 K) which acts as a transition phase depicting a switch from heterogeneous to homogeneous reaction path initiated by gas-phase reactions of aluminum monoxide (AlO) along with facile hydrogen abstraction from JP-10 and successive decomposition of these JP-10 radicals to hydrocarbon radical fragments, and a **high-temperature regime** (1250−1450 K) driven by the unimolecular decomposition of JP-10 by collision with helium atoms and contributions from gas-phase reactions initiated between JP-10 and aluminum monoxide (AlO). These three regimes are summarized in Scheme 2.

In the **low-temperature regime**, the detection of oxygenated radicals and molecules at temperatures as low as 650 K in the presence of AlNPs reveals a temperature-dependent active oxygen chemistry of the aluminum oxide layer going hand in hand with a transfer of oxygen from the inorganic oxide layer to the organic, oxygen-containing radicals and molecules. Considering the lack of any aluminum oxide species in the gas phase at these low temperatures, aluminum monoxide (AlO) radicals cannot be involved in any gas-phase oxidation process from 650 to 950 K. Consequently, the oxygen incorporated in the gas-phase products—at least in the above-mentioned temperature range—must originate from the aluminum oxide layer. This necessitates a surface-mediated oxidation of adsorbed JP-10 molecules on the aluminum oxide layer in the low-temperature decomposition and oxidation stage of JP-10. Overall, the low-temperature regime from 650 K to about 1050 K is characterized by a facile oxidation process of JP-10 driven by the aluminum oxide surface.

Scheme 2. Distinct Stages of Thermal Decomposition of JP-10 by Aluminum Nanoparticles (AlNPs) Involving Heterogeneous Surface−Gas-Phase Chemistries along with the Fate of the Alumina Oxide Layer and the Aluminum Core as a Function of Temperature

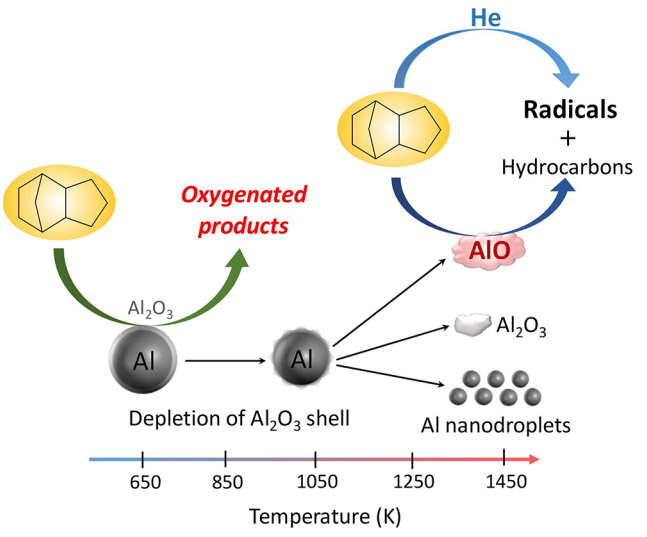

The emergence of aluminum monoxide radicals (AlO) hints to a gas-phase chemistry initiated by aluminum monoxide radicals in the **medium-temperature regime** commencing at about 1050 K. The release of aluminum monoxide (AlO) into the gas phase might be driven by the melting of the aluminum core beyond 933 K[48] leading to the expansion of the core, inducing significant stress on the alumina oxide shell[49−51] causing it to rupture, hence accumulating aluminum oxide shell material along with aluminum nanodroplets. Alternatively, the exposed reactive aluminum core could abstract oxygen from the oxygenated organics. Since in the blank experiment, i.e., heating AlNPs over a temperature range from 300 to 1450 K, no gas-phase aluminum monoxide radicals (AlO) were observed, the abstraction of oxygen from the oxygenated organics by the exposed reactive aluminum core represents a plausible route of formation of aluminum monoxide. Note that previous studies suggest that aluminum monoxide only forms at high temperatures exceeding 2000 K.[52] Once released into the gas phase, previous electronic structure calculations disclosed facile hydrogen abstraction pathways from gas-phase JP-10 by aluminum monoxide radicals (AlO)[27] followed by unimolecular decomposition of the initial hydrocarbon radicals generated to the detected hydrocarbon radicals and molecules (Figure 2B and Figure S4).[29] The reactions of aluminum monoxide radical (AlO) with JP-10 ($C_{10}H_{16}$) to form six distinct JP-10 carbon-centered radicals ($C_{10}H_{15}$) plus aluminum monohydroxide (AlOH) are exoergic by 52−98 kJ mol^{-1} and are initiated by the formation of van der Waals complexes in the entrance channel, which are weakly stabilized by 8−48 kJ mol^{-1}.[27] These long-range complexes undergo hydrogen atom abstraction through transition states located only between 4 and 20 kJ mol^{-1} above the separated reactants. Even at 1050 K, these low-lying transition states can be overcome easily yielding van der Waals complexes between the JP-10 radical ($C_{10}H_{15}$) and aluminum monohydroxide (AlOH)

https://doi.org/10.1021/acs.jpclett.3c02532
J. Phys. Chem. Lett. 2023, 14, 9341−9350

strongly stabilized by −71 to −109 kJ mol^{-1} prior to forming the separated JP-10 radical ($C_{10}H_{15}$) and aluminum monohydroxide (AlOH) products. The gas-phase formation of these radicals initiates a complex chain of their decomposition, yielding eventually the experimentally detected hydrocarbons along with their radicals (Figures 4).[29]

As the temperature exceeds 1250 K, that is, in the **high-temperature regime**, the mass spectra of the decomposition products of JP-10 in the presence of AlNPs (Figure 1, Figure S7) are nearly identical to those of helium seeded JP-10 at temperatures of 1500 K, except for the appearance of a few oxygenated products and enhanced decomposition of JP-10 for the present system. However, at 1450 K the oxygenated products diminish significantly. These findings suggest that at temperatures near and exceeding 1450 K, the gas-phase processes are driven largely by decomposition of JP-10 induced by collision with helium atoms (He) from the carrier gas along with facile reaction of aluminum monoxide (AlO) with JP-10. The latter channel may account for the higher extent of degradation of JP-10 in comparison to the existing gas-phase pyrolysis of pristine JP-10.

Overall, our study of the decomposition and oxidation of *exo*-tetrahydrodicyclopentadiene (JP-10, $C_{10}H_{16}$) in the presence of aluminum oxide (Al_2O_3)-coated aluminum nanoparticles (AlNPs) reveals three distinct, temperature-dependent phases with diverse roles of the AlNPs to the underlying chemistry. The **low-temperature regime** is driven by surface-mediated heterogeneous reactions between JP-10 and the oxide layer of the AlNPs leading to JP-10 radicals along with oxygenated degradation products. The **medium-temperature regime** is essentially a transition phase from heterogeneous to the homogeneous gas-phase reaction pathway involving aluminum monoxide (AlO) with JP-10 forming distinct JP-10 radicals, which then undergo decomposition to hydrocarbon molecules and their radicals. Finally, in the **high-temperature regime**, the decomposition dynamics of JP-10 are largely driven by the high-temperature collisions with the helium atoms and from facile gas-phase reactions initiated through the abstraction of hydrogen from JP-10 by aluminum monoxide (AlO). The decline of the yields of the oxidized products with rising temperature above 1050 K likely resulted from their lower thermal stabilities, the lack of available oxidizer due to a transition from a heterogeneous surface chemistry (low-temperature regime) to homogeneous gas-phase chemistry (medium-temperature regime), and/or collision-induced thermal decomposition with helium. Hence, the key advantage of AlNP additives to JP-10 is not only limited to lowering the operational temperature of jet engines by at least 150 K for a complete decomposition of JP-10 to occur but also the facile and robust applicability in engine environments, where essentially no pretreatment to remove the alumina passivation layer is required. The immediate next undertaking in this area of study is to address the reactivity and efficiency of alumina-coated AlNPs in the decomposition of JP-10 in synthetic air, that is, in the presence of molecular oxygen, mimicking the air-breathing propulsion system. It is also of fundamental interest to determine how the AlNPs without any coating would influence the decomposition chemistry of JP-10.

To summarize, the work presented here represents a very first step toward the systematic understanding of the decomposition of JP-10 molecules in the presence of AlNPs. Intuitively, the active oxygen chemistry can further be facilitated by substituting the presumed "inert" alumina shell through a layer of more reactive, oxygen-releasing oxidizer material. Recent research suggests that aluminum iodate hexahydrate ($[Al(H_2O)_6](IO_3)_3(HIO_3)_2$; AIH) could act as such a replacement of the aluminum oxide layer of AlNPs with AIH liberating oxidizers such as oxygen (O_2) and iodine (I_2) upon its decomposition at temperatures as low as 600 K.[53−57] Therefore, a series of comparative systematic studies of the thermal degradation of JP-10 in the presence of AIH-coated AlNPs is warranted to untangle the complexity of surface-mediated reactions which dictate the actual course of the decomposition dynamics.

■ ASSOCIATED CONTENT

Supporting Information

The Supporting Information is available free of charge at https://pubs.acs.org/doi/10.1021/acs.jpclett.3c02532.

Experimental methods, photoionization efficiency curves of the hydrocarbon products, mass spectra recorded at 15.4 eV, temperature-dependent abundances of water due to thermal decomposition of JP-10 by AlNPs, comparison of the mass spectra obtained upon thermal decomposition of JP-10 without any additive at 1500 K and with AlNPs at 1250 K, compilation of the products observed in the thermal decomposition of JP-10 on AlNPs, and quantification of temperature-dependent oxygen uptake coefficient from alumina oxide shell (PDF)

■ AUTHOR INFORMATION

Corresponding Authors

Musahid Ahmed − *Chemical Sciences Division, Lawrence Berkeley National Laboratory, Berkeley, California 94720, United States;* orcid.org/0000-0003-1216-673X; Email: mahmed@lbl.gov

Michelle L. Pantoya − *Mechanical Engineering Department, Texas Tech University, Lubbock, Texas 79409, United States;* orcid.org/0000-0003-0299-1832; Email: michelle.pantoya@ttu.edu

Ralf I. Kaiser − *Department of Chemistry, University of Hawai'i at Manoa, Honolulu, Hawaii 96822, United States;* orcid.org/0000-0002-7233-7206; Email: ralfk@hawaii.edu

Authors

Souvick Biswas − *Department of Chemistry, University of Hawai'i at Manoa, Honolulu, Hawaii 96822, United States*

Dababrata Paul − *Department of Chemistry, University of Hawai'i at Manoa, Honolulu, Hawaii 96822, United States*

Chao He − *Department of Chemistry, University of Hawai'i at Manoa, Honolulu, Hawaii 96822, United States*

Nureshan Dias − *Chemical Sciences Division, Lawrence Berkeley National Laboratory, Berkeley, California 94720, United States*

Complete contact information is available at: https://pubs.acs.org/10.1021/acs.jpclett.3c02532

Notes

The authors declare no competing financial interest.

■ ACKNOWLEDGMENTS

The Hawaii and the Texas groups were supported by the United States Office of Naval Research (ONR) under Contract

Number N00014-22-1-2010 and N00014-22-1-2006, respectively. M.A. and N.D. are supported by the Director, Office of Science, Office of Basic Energy Sciences, of the U.S. Department of Energy under Contract No. DE-AC02-05CH11231, through the Gas Phase Chemical Physics program of the Chemical Sciences Division. The ALS is supported through the same contract.

REFERENCES

(1) Jing, Q.; Wang, D.; Shi, C. Effects of Aluminum Powder Additives on Deflagration and Detonation Performance of JP-10/DEE Mixed Fuel Under Weak and Strong Ignition Conditions. *Appl. Energy* **2023**, *331*, No. 120477.

(2) Luo, Y.; Xu, X.; Zou, J.-J.; Zhang, X. Combustion of JP-10-Based Slurry with Nanosized Aluminum Additives. *J. Propuls. Power* **2016**, *32*, 1167−1177.

(3) Liu, L.; Zhang, Q.; Shen, S.; Li, D.; Lian, Z.; Wang, Y. Evaluation of Detonation Characteristics of Aluminum/JP-10/Air Mixtures at Stoichiometric Concentrations. *Fuel* **2016**, *169*, 41−49.

(4) Liu, J. Z.; Chen, B. H.; Wu, T. T.; Yang, W. J.; Zhou, J. H. Ignition and Combustion Characteristics and Agglomerate Evolution Mechanism of Aluminum in nAl/JP-10 Nanofluid Fuel. *J. Therm. Anal.* **2019**, *137*, 1369−1379.

(5) Chen, B. H.; Liu, J. Z.; Li, H. P.; Yang, W. J.; Cen, K. F. Laser Ignition and Combustion Characteristics of Al/JP-10 Nanofluid Droplet. *J. Therm. Anal.* **2019**, *135*, 925−934.

(6) E, X.-T.-F.; Zhang, L.; Wang, F.; Zhang, X.; Zou, J.-J. Synthesis of Aluminum Nanoparticles as Additive to Enhance Ignition and Combustion of High Energy Density Fuels. *Front. Chem. Sci. Eng.* **2018**, *12*, 358−366.

(7) E, X.-t.-f.; Pan, L.; Wang, F.; Wang, L.; Zhang, X.; Zou, J.-J. Al-Nanoparticle-Containing Nanofluid Fuel: Synthesis, Stability, Properties, and Propulsion Performance. *Ind. Eng. Chem. Res.* **2016**, *55*, 2738−2745.

(8) Javed, I.; Baek, S. W.; Waheed, K. Autoignition and Combustion Characteristics of Heptane Droplets with the Addition of Aluminium Nanoparticles at Elevated Temperatures. *Combust. Flame* **2015**, *162*, 191−206.

(9) Allen, C.; Mittal, G.; Sung, C.-J.; Toulson, E.; Lee, T. An Aerosol Rapid Compression Machine for Studying Energetic-Nanoparticle-Enhanced Combustion of Liquid Fuels. *Proc. Combust. Inst* **2011**, *33*, 3367−3374.

(10) Brotton, S. J.; Malek, M. J.; Anderson, S. L.; Kaiser, R. I. Effects of Acetonitrile-Assisted Ball-Milled Aluminum Nanoparticles on the Ignition of Acoustically Levitated exo-Tetrahydrodicyclopentadiene (JP-10) Droplets. *Chem. Phys. Lett.* **2020**, *754*, No. 137679.

(11) Lucas, M.; Brotton, S. J.; Min, A.; Woodruff, C.; Pantoya, M. L.; Kaiser, R. I. Effects of Size and Prestressing of Aluminum Particles on the Oxidation of Levitated exo-Tetrahydrodicyclopentadiene Droplets. *J. Phys. Chem. A* **2020**, *124*, 1489−1507.

(12) Lucas, M.; Brotton, S. J.; Min, A.; Pantoya, M. L.; Kaiser, R. I. Oxidation of Levitated exo-Tetrahydrodicyclopentadiene Droplets Doped with Aluminum Nanoparticles. *J. Phys. Chem. Lett.* **2019**, *10*, 5756−5763.

(13) Kuo, K. K.; Risha, G. A.; Evans, B. J.; Boyer, E. Potential Usage of Energetic Nano-sized Powders for Combustion and Rocket Propulsion. *MRS Online Proceedings Library* **2003**, *800*, 39−50.

(14) Yetter, R. A.; Risha, G. A.; Son, S. F. Metal Particle Combustion and Nanotechnology. *Proc. Combust. Inst* **2009**, *32*, 1819−1838.

(15) Granier, J. J.; Pantoya, M. L. Laser Ignition of Nanocomposite Thermites. *Combust. Flame* **2004**, *138*, 373−383.

(16) Karmakar, S.; Wang, N.; Acharya, S.; Dooley, K. M. Effects of Rare-Earth Oxide Catalysts on The Ignition and Combustion Characteristics of Boron Nanoparticles. *Combust. Flame* **2013**, *160*, 3004−3014.

(17) Ojha, P. K.; Prabhudeva, P.; Karmakar, S.; Maurya, D.; Sivaramakrishna, G. Combustion Characteristics of JP-10 Droplet Loaded with Sub-Micron Boron Particles. *Exp. Therm. Fluid Sci.* **2019**, *109*, No. 109900.

(18) Ojha, P. K.; Karmakar, S. Boron for Liquid Fuel Engines-A Review on Synthesis, Dispersion Stability in Liquid Fuel, and Combustion Aspects. *Prog. Aerosp. Sci.* **2018**, *100*, 18−45.

(19) DeLisio, J. B.; Hu, X.; Wu, T.; Egan, G. C.; Young, G.; Zachariah, M. R. Probing the Reaction Mechanism of Aluminum/Poly(vinylidene fluoride) Composites. *J. Phys. Chem. B* **2016**, *120*, 5534−5542.

(20) Walzel, R. K.; Levitas, V. I.; Pantoya, M. L. Aluminum Particle Reactivity As a Function of Alumina Shell Structure: Amorphous versus Crystalline. *Powder Technol.* **2020**, *374*, 33−39.

(21) Padhye, R.; McCollum, J.; Korzeniewski, C.; Pantoya, M. L. Examining Hydroxyl−Alumina Bonding toward Aluminum Nanoparticle Reactivity. *J. Phys. Chem. C* **2015**, *119*, 26547−26553.

(22) Malek, M. I.; Wu, C.-C.; Walck, S. D.; Pantoya, M. L. Hydration of Alumina (Al_2O_3) toward Advancing Aluminum Particles for Energy Generation Applications. *Colloids Surf. A: Physicochem. Eng.* **2022**, *652*, No. 129740.

(23) Pantoya, M. L.; Dean, S. W. The Influence of Alumina Passivation on Nano-Al/Teflon Reactions. *Thermochim. Acta* **2009**, *493*, 109−110.

(24) Gesner, J.; Pantoya, M. L.; Levitas, V. I. Effect of Oxide Shell Growth on Nano-Aluminum Thermite Propagation Rates. *Combust. Flame* **2012**, *159*, 3448−3453.

(25) Padhye, R.; Aquino, A. J. A.; Tunega, D.; Pantoya, M. L. Effect of Polar Environments on the Aluminum Oxide Shell Surrounding Aluminum Particles: Simulations of Surface Hydroxyl Bonding and Charge. *ACS Appl. Mater. Interfaces* **2016**, *8*, 13926−13933.

(26) Padhye, R.; Aquino, A. J. A.; Tunega, D.; Pantoya, M. L. Fluorination of an Alumina Surface: Modeling Aluminum−Fluorine Reaction Mechanisms. *ACS Appl. Mater. Interfaces* **2017**, *9*, 24290−24297.

(27) Brotton, S. J.; Perera, S. D.; Misra, A.; Kleimeier, N. F.; Turner, A. M.; Kaiser, R. I.; Palenik, M.; Finn, M. T.; Epshteyn, A.; Sun, B.-J.; et al. Combined Spectroscopic and Computational Investigation on the Oxidation of exo-Tetrahydrodicyclopentadiene (JP-10; $C_{10}H_{16}$) Doped with Titanium−Aluminum−Boron Reactive Metal Nanopowder. *J. Phys. Chem. A* **2022**, *126*, 125−144.

(28) Jin, Y.; Dou, S.; Yang, Q.; Xu, X.; Fu, Q.; Pan, L. Performance Characteristics of a Scramjet Engine Using JP-10 Fuel Containing Aluminum Nanoparticles. *Acta Astronaut.* **2021**, *185*, 70−77.

(29) Zhao, L.; Yang, T.; Kaiser, R. I.; Troy, T. P.; Xu, B.; Ahmed, M.; Alarcon, J.; Belisario-Lara, D.; Mebel, A. M.; Zhang, Y.; et al. A Vacuum Ultraviolet Photoionization Study on High-Temperature Decomposition of JP-10 (exo-Tetrahydrodicyclopentadiene). *Phys. Chem. Chem. Phys.* **2017**, *19*, 15780−15807.

(30) Kohn, D. W.; Clauberg, H.; Chen, P. Flash Pyrolysis Nozzle for Generation of Radicals in a Supersonic Jet Expansion. *Rev. Sci. Instrum.* **1992**, *63*, 4003−4005.

(31) Zhang, F.; Kaiser, R. I.; Golan, A.; Ahmed, M.; Hansen, N. A VUV Photoionization Study of the Combustion-Relevant Reaction of the Phenyl Radical (C_6H_5) with Propylene (C_3H_6) in a High Temperature Chemical Reactor. *J. Phys. Chem. A* **2012**, *116*, 3541−3546.

(32) Parker, D. S. N.; Kaiser, R. I. On the Formation of Nitrogen-Substituted Polycyclic Aromatic Hydrocarbons (NPAHs) in Circumstellar and Interstellar Environments. *Chem. Soc. Rev.* **2017**, *46*, 452−463.

(33) Photonionization Cross Section Database (Version 2.0); National Synchrotron Radiation Laboratory; Hefei, China, http://flame.nsrl.ustc.edu.cn/database/.

(34) Kaiser, R. I.; Zhao, L.; Lu, W.; Ahmed, M.; Krasnoukhov, V. S.; Azyazov, V. N.; Mebel, A. M. Unconventional Excited-State Dynamics in the Concerted Benzyl (C_7H_7) Radical Self-Reaction to anthracene ($C_{14}H_{10}$). *Nat. Commun.* **2022**, *13*, 786.

(35) Zhang, T.; Tang, X. N.; Lau, K. C.; Ng, C. Y.; Nicolas, C.; Peterka, D. S.; Ahmed, M.; Morton, M. L.; Ruscic, B.; Yang, R.; et al. Direct Identification of Propargyl Radical in Combustion Flames by

https://doi.org/10.1021/acs.jpclett.3c02532
J. Phys. Chem. Lett. 2023, 14, 9341−9350

Vacuum Ultraviolet Photoionization Mass Spectrometry. *J. Chem. Phys.* **2006**, *124*, No. 074302.
(36) Huang, C.; Wei, L.; Yang, B.; Wang, J.; Li, Y.; Sheng, L.; Zhang, Y.; Qi, F. Lean Premixed Gasoline/Oxygen Flame Studied with Tunable Synchrotron Vacuum UV Photoionization. *Energy Fuels* **2006**, *20*, 1505−1513.
(37) Meloni, G.; Selby, T. M.; Goulay, F.; Leone, S. R.; Osborn, D. L.; Taatjes, C. A. Photoionization of 1-Alkenylperoxy and Alkylperoxy Radicals and a General Rule for the Stability of Their Cations. *J. Am. Chem. Soc.* **2007**, *129*, 14019−14025.
(38) Savee, J. D.; Sztáray, B.; Welz, O.; Taatjes, C. A.; Osborn, D. L. Valence Photoionization and Autoionization of the Formyl Radical. *J. Phys. Chem. A* **2021**, *125*, 3874−3884.
(39) Qi, F. E. I.; McIlroy, A. Identifying Combustion Intermediates via Tunable Vacuum Ultraviolet Photoionization Mass Spectrometry. *Combust. Sci. Technol.* **2005**, *177*, 2021−2037.
(40) Parker, D. S. N.; Kaiser, R. I.; Troy, T. P.; Kostko, O.; Ahmed, M.; Mebel, A. M. Toward the Oxidation of the Phenyl Radical and Prevention of PAH Formation in Combustion Systems. *J. Phys. Chem. A* **2015**, *119*, 7145−7154.
(41) Wu, X.; Zhou, X.; Hemberger, P.; Bodi, A. The Ionization Energy of the Vinyl Radical: A Mexican Standoff with a Happy Ending. *Phys. Chem. Chem. Phys.* **2019**, *21*, 22238−22247.
(42) Prendergast, M. B.; Kirk, B. B.; Savee, J. D.; Osborn, D. L.; Taatjes, C. A.; Hemberger, P.; Blanksby, S. J.; da Silva, G.; Trevitt, A. J. Product Detection Study of the Gas-Phase Oxidation of Methylphenyl Radicals Using Synchrotron Photoionisation Mass Spectrometry. *Phys. Chem. Chem. Phys.* **2019**, *21*, 17939−17949.
(43) Hunter, E. P. L.; Lias, S. G. Evaluated Gas Phase Basicities and Proton Affinities of Molecules: An Update. *J. Phys. Chem. Ref. Data* **1998**, *27*, 413−656.
(44) Potts, A. W.; Fattahallah, G. H. High-resolution Ultraviolet Photoelectron Spectroscopy of CO_2, COS and CS_2. *J. Phys. B: At. Mol. Opt. Phys.* **1980**, *13*, 2545.
(45) Schweig, A.; Vermeer, H.; Weidner, U. A Photoelectron Spectroscopic Study of Keto-Enol Tautomerism in Acetylacetones - A New Application of Photoelectron Spectroscopy. *Chem. Phys. Lett.* **1974**, *26*, 229−233.
(46) Hildenbrand, D. L. Dissociation Energies of the Molecules AlO and Al_2O. *Chem. Phys. Lett.* **1973**, *20* (1), 127−129.
(47) Dinda, S.; Vuchuru, K.; Konda, S.; Uttaravalli, A. N. Heat Management in Supersonic/Hypersonic Vehicles Using Endothermic Fuel: Perspective and Challenges. *ACS Omega* **2021**, *6*, 26741−26755.
(48) Patel, V. K.; Joshi, A.; Kumar, S.; Rathaur, A. S.; Katiyar, J. K. Molecular Combustion Properties of Nanoscale Aluminum and Its Energetic Composites: A Short Review. *ACS Omega* **2021**, *6*, 17−27.
(49) Levitas, V. I.; Asay, B. W.; Son, S. F.; Pantoya, M. Mechanochemical Mechanism for Fast Reaction of Metastable Intermolecular Composites Based on Dispersion of Liquid Metal. *J. Appl. Phys.* **2007**, *101*, No. 083524.
(50) Levitas, V. I.; Pantoya, M. L.; Dikici, B. Melt Dispersion versus Diffusive Oxidation Mechanism for Aluminum Nanoparticles: Critical Experiments and Controlling Parameters. *Appl. Phys. Lett.* **2008**, *92*, No. 011921.
(51) Wu, B.; Wu, F.; Wang, P.; He, A.; Wu, H. Ignition and Combustion of Hydrocarbon Fuels Enhanced by Aluminum Nanoparticle Additives: Insights from Reactive Molecular Dynamics Simulations. *J. Phys. Chem. C* **2021**, *125*, 11359−11368.
(52) Lynch, P.; Fiore, G.; Krier, H.; Glumac, N. Gas-Phase Reaction in Nanoaluminum Combustion. *Combust. Sci. Technol.* **2010**, *182*, 842−857.
(53) Rizzo, G. L.; Biswas, S.; Antonov, I.; Miller, K. K.; Pantoya, M. L.; Kaiser, R. I. Exotic Inverse Kinetic Isotopic Effect in the Thermal Decomposition of Levitated Aluminum Iodate Hexahydrate Particles. *J. Phys. Chem. Lett.* **2023**, *14*, 2722−2730.
(54) Kalman, J.; Smith, D. K.; Miller, K. K.; Bhattacharia, S. K.; Bratton, K. R.; Pantoya, M. L. A Strategy for Increasing the Energy Release Rate of Aluminum by Replacing the Alumina Passivation Shell with Aluminum Iodate Hexahydrate (AIH). *Combust. Flame* **2019**, *205*, 327−335.
(55) Smith, D. K.; McCollum, J.; Pantoya, M. L. Effect of Environment on Iodine Oxidation State and Reactivity with Aluminum. *Phys. Chem. Chem. Phys.* **2016**, *18*, 11243−11250.
(56) Smith, D. K.; Bello, M. N.; Unruh, D. K.; Pantoya, M. L. Synthesis and Reactive Characterization of Aluminum Iodate Hexahydrate Crystals $[Al(H_2O)_6](IO_3)_3(HIO_3)_2$. *Combust. Flame* **2017**, *179*, 154−156.
(57) Smith, D. K.; Unruh, D. K.; Wu, C.-C.; Pantoya, M. L. Replacing the Al_2O_3 Shell on Al Particles with an Oxidizing Salt, Aluminum Iodate Hexahydrate. Part I: Reactivity. *J. Phys. Chem. C* **2017**, *121*, 23184−23191.

https://doi.org/10.1021/acs.jpclett.3c02532
J. Phys. Chem. Lett. 2023, 14, 9341−9350